1   Multiconfiguration electromagnetic induction survey for paleochannel internal structure

2   imaging: a case study in the alluvial plain of the river Seine, France.

4   Fayçal Rejiba[1], Cyril Schamper[1], Antoine Chevalier[1], Benoit Deleplancque[2],

5   Gaghik Hovhannissian[3], Julien Thiesson[1] & Pierre Weill[4]

7   [1]*Sorbonne Université – UPMC Univ Paris 06, CNRS, UMR 7619 METIS, Paris, France*

8   [2] *UMR CNRS 7423 - Ecole Polytechnique de l'Université François Rabelais de Tours, 35*

9   *allée Ferdinand de Lesseps - 37200 Tours.*

10   [3] *North Delegation of the Institute of Research for Development (IRD), UMR 242 iEES Paris*

11   *(Institute of Ecology and Environmental Sciences), IRD/CNRS/UPMC/INRA/UPEC/Univ.*

12   *Paris Diderot, 32 av. H. Varagnat, 93143, Bondy, France*

13   [4]*Normandie Univ, UNICAEN, UNIROUEN CNRS, Morphodynamique Continentale et*

14   *Côtière, 14000 Caen, France*

15   *Corresponding author: Fayçal Rejiba (faycal.rejiba@upmc.fr)*

16   *Running title:* Geophysical Investigations of a Paleochannel

Abstract

The La Bassée floodplain area is a large groundwater reservoir controlling most of the water exchanged between local aquifers and hydrographic networks within the Seine River Basin (France). Preferential flows depend essentially on the heterogeneity of alluvial plain infilling, whose characteristics are strongly influenced by the presence of mud plugs (paleomeander clayey infilling). These mud plugs strongly contrast with the coarse sand material that composes most of the alluvial plain, and can create permeability barriers to groundwater flows. A detailed knowledge of the global and internal geometry of such paleomeanders can thus lead to a comprehensive understanding of the long-term hydrogeological processes of the alluvial plain. A geophysical survey based on the use of electromagnetic induction was performed on a wide paleomeander, situated close to the city of Nogent-sur-Seine in France. In the present study we assess the advantages of combining several spatial offsets, together with both vertical and horizontal dipole orientations (6 apparent conductivities), thereby mapping not only the spatial distribution of the paleomeander derived from LIDAR data, but also its vertical extent and internal variability.

1. Introduction

Dipolar source electromagnetic induction (EMI) techniques are frequently used for critical zone mapping, which can be applied to the delineation of shallow heterogeneities, thereby improving conceptual models used to explain the processes affecting a wide range of sedimentary environments. This mapping technique is very effective for environments in which the spatial structure has strongly contrasted electromagnetic (EM) properties especially that of interpreted electrical conductivity (EC).

45   Since the seminal work of Rhoades (Rhoades et al., 1976) much research has been

46   conducted to link the petrophysical and hydrodynamic soil properties to the apparent

47   electrical conductivity (EC_a). EC_a is affected by numerous parameters (Friedman, 2005)

48   whose major ones can be separated into three categories: (1) the bulk soil properties (porosity,

49   water content, structure); (2) the type of solid particle (geometry, distribution and cation

50   exchange capacity) mainly related to the clay content; and, (3) environmental factors (EC of

51   water, temperature,…). The clay infilling of paleochannels, and the deposition of alternate

52   layers of conductive (clayey) and resistive (sandy) material in alluvial plain systems, are

53   examples of natural geophysical processes having contrasted EM properties.

54   EMI measurements have previously been applied to the imaging of conductive fine-

55   grained paleomeander infilling, produced by meander neck cutoff or river avulsion, which can

56   form permeability barriers with complex geometries (e.g. Miall, 1988; Fitterman et al., 1991;

57   Jordan and Prior, 1992; De Smedt at al., 2011). In addition to providing detailed local

58   information on alluvial plain heterogeneities, which can be applied to the study of aquifer-

59   river exchanges (Flipo et al. 2014), the estimation of the geometry of the Seine river

60   paleochannels can provide valuable insight into its paleo-hydrology, as well as physical

61   transformations resulting from climatic fluctuations during the Late Quaternary.

62   EMI devices are increasingly used for a large number of near-surface geophysical

63   applications, as a consequence of their ability to produce mapping of EC_a over extended areas

64   and at different depths. The main issue of EMI concerns the quantitative mapping of the

65   vertical variations of EC, obtained after multilayer inversion of EC_a, because of the limited

66   number of measurements at different depths (i.e. source-receiver offsets). Despite the

67   spreading use of multiple-frequency and multiple-coil EMI instruments compared to the

68   classic twin coils configuration, a way to overcome this issue is, at least to constrain, and at

69   best to calibrate multilayer inversion of EMI measurements against ERI (electrical resistivity

70   imagery) profiling. A very large body of scientific literature has been published on the study

71   and use of near-surface electromagnetic geophysics, especially in the frequency domain, as

72   described by Everett (2012).

73   By design, an EMI system energizes a transmitter coil with a monochromatic

74   oscillating current, and the oscillating magnetic field produced by this current induces an

75   oscillating voltage response in the receiver coil. The voltage response measured in the

76   absence of any conductive structure is used as a standard reference. However, the magnetic

77   field oscillations are distorted by the presence of nearby conductive structures, such that the

78   voltage signal induced in the receiver coil experiences a shift in amplitude and phase with

79   respect to that observed in the standard reference. This shift can be conveniently represented

80   by a complex number, comprising quadrature (or imaginary) and in-phase (or real)

81   components, which can be interpreted in terms of EC_a (from the quadrature or out-of-phase

82   part) and depth of investigation (DOI) (Huang, 2005). A comprehensive and more detailed

83   description of the EMI principles can be found in (Nabighian, 1988a, 1988b).

84   Although EMI systems were initially used as mapping tools, and were designed to

85   measure the lateral variability of EC associated with a single DOI, the measurements they

86   provide are now generally interpreted to provide information as a function of depth, albeit

87   down to only relatively shallow depths. This interpretation relies on the fact that, for a given

88   soil model, one specific DOI is defined by four device setup parameters: (1) the offset

89   between the transmitter and receiver magnetic dipole; (2) the orientation of the dipole pair; (3)

90   the frequency of the transmitter current oscillations; and, (4) the instrument height above the

91   ground. An EMI survey during which at least one of these parameters is varied can thus be

92   used to resolve depth-related variations of EC. This distribution can be retrieved by solving an

93 inverse problem, which is derived from a large number of applications (e.g. Tabbagh, 1986;

94 Spies, 1989; Nabighian, 1988b; Schamper et al., 2012).

95   The physical model used in the inversion procedure must be suitably adapted to the

96 electromagnetic properties of the surveyed ground. In the case of a medium characterized by

97 typical conductive properties (e.g. low, non-ferromagnetic materials), at a low induction

98 number the quadrature response is interpreted in terms of the apparent ground resistivity,

99 which to a first order approximation varies linearly with the quadrature response (McNeill,

100 1980). In a resistive (EM effects other than induction become non negligible) or highly

101 conductive (low-induction number assumption is no longer valid) environment, such as that

102 mapped in the present study, the EMI recordings, in particular their in-phase component, must

103 be interpreted within the specific measurement context. One must then take into account, in

104 addition to the EC, the magnetic susceptibility and viscosity, as well as the dielectric

105 permittivity of the local environment, especially if this one is resistive (e.g. Simon et al.,

106 2015, Benech et al., 2016).

107   The present study focuses on the La Bassée alluvial plain, a zone located in the

108 southern part of the Seine basin, 2 km to the west of Nogent-sur-Seine (France). The

109 geophysical campaign has been performed during 3 days of good weather in June during a

110 low water period. The use of geophysical exploration for this investigation is of significant

111 importance, since it should pave the way for the paleo-hydrological reconstruction of the

112 Seine River (estimation of its transversal geometry and paleo-discharge).

113   The aim of this study is to delineate the geometry of a paleochannel (i.e. its thickness

114 and width), using a state-of-the-art 1D inversion routine applied to EMI EC_a measurements.

115 The inverted data consist in a set of EMI measurements implemented with (1) three different

116 offsets, and, (2) for two dipole configurations: horizontal (HCP) and vertical (VCP).

117   Following a description of the study area, we present the technique used to calibrate

118 the EMI measurements, which relies on reference ERI (Electrical Resistivity Imaging)

119 measurements and an auger sounding profile. The EMI inversion is then constrained to limit

120 the solution space to images that are consistent with the observations provided by the ERI and

121 auger soundings. To this end, a local three-layer model is derived with fixed conductivities,

122 and is then introduced into the inversion routine for each position of the surveyed area. The

123 thicknesses of the soil and conductive filling, corresponding to the presumed paleochannel,

124 are determined through the use of an inversion algorithm.

125   **2.   Description of the study area**

126 The study site is located within a portion of the Seine River alluvial plain (locally named

127 "Bassée"), approximately one hundred kilometers upstream of Paris (France), between the

128 confluence of the Seine and Aube rivers to the North-East, and the confluence of the Seine

129 and Yonne rivers to the South-West (Figure 1). This 60 kilometer-long, 4 kilometer-wide

130 alluvial plain constitutes a heterogeneous sedimentary environment, resulting from the

131 development of the Seine River during the Middle and Late Quaternary.

132   Cartographic studies of this area have been carried out in the past, using

133 geomorphological and sedimentological techniques (Mégnien, 1965; Caillol et al., 1977;

134 Mordant, 1992; Berger et al., 1995; Deleplancque, 2016), thus allowing the broad-scale

135 distribution and chronology of the location of the main Middle and Late Quaternary alluvial

136 sheets to be estimated.

137   In addition, the French Geological Survey (BRGM) has compiled a database of more

138   than 500 soundings, which are uniformly distributed over the Bassée alluvial plain, and most

139   of which reached the Cretaceous chalky substrate. A detailed analysis and interpretation of

140   this database has allowed the substratum morphology to be reconstructed, the alluvial infilling

141   thickness to be evaluated, and a preliminary quantitative analysis of the sedimentary facies

142   distribution to be determined (Deleplancque, 2016). The maximum thickness of the alluvial

143   infilling is thus known to lie between 6 and 8 m.

144   Geophysical investigations of gravel pits (after removal of the conductive topsoil)

145   were carried out using ground-penetrating radar (Deleplancque, 2016), and have contributed

146   to the characterization of the sedimentary contrast of the sand bar architecture, between the

147   Weichselian and Holocene deposits. The Weichselian deposits are typical of braided fluvial

148   systems, with fluvial bars of moderate extent (< 50 m) truncated by large erosional surfaces.

149   The thickness of the preserved braid-bars rarely exceeds 1.5 m. The Holocene architecture is

150   associated mainly with single-channel meandering fluvial systems, characterized by thick

151   point-bar deposits (> 4 m) with a lateral extent of several hundred meters, sometimes

152   interrupted by clayey paleochannel infillings. Traces of small sinuous channels, probably

153   using the paths of former Weichseilian braided channels, are also identified at the edge of the

154   alluvial plain.

155   Aerial photography and a LIDAR (laser detection and ranging) topographic survey

156   (Figure 2) have been used to characterize the paleochannel plan-view morphologies (style,

157   width, meander wavelength), of the most recent (Holocene) meandering alluvial sheets in this

158   area (Deleplancque, 2016). These measurements were complemented by auger soundings and

159   ^{14}C dating of organic debris or bulk sediment (peat), in order to determine a time-frame for

160   the development of the Seine meanders and to allow these changes to be compared with other

161 regional studies (e.g. Antoine et al. 2003; Pastre et al., 2003). The paleochannel investigated

162 in this study is located 2 km to the South-West of Nogent-sur-Seine (covered by a grassy

163 meadow) and is characterized by larger dimensions than the present-day Seine River. Its

164 width is estimated to lie between 150 and 300 m, with a meander wavelength between 2 and

165 3 km. According to the alluvial sheet analysis and the dating of organic material in the mud-

166 plug of the abandoned meander, it is very likely that this paleochannel was active between the

167 Late Glacial and Preoboreal periods (Deleplancque, 2016).

168   **3. Field survey and measurement setup**
169

170 The survey coordinates were determined through the use of a LIDAR map (Deleplancque,

171 2016), combined with the analysis of a series of auger soundings made along a reference

172 transect of almost 400 m in length (Figure 2 and Figure 3). The lateral extent of the meander

173 was delineated using an EMI system (CMD explorer) produced by GF instruments s.r.o., with

174 non-regular gridding and non-perfect overlapping inside the same area.

175 **3.1 ERI and hand auger soundings results**
176   A total of 13 hand auger soundings down to a maximum depth of 2.4 m (Figure 4),

177 were made along the reference profile. Some of these soundings did not reach the base of the

178 paleomeander mud-plug (clay / gravel transition), suggesting that the maximum depth of the

179 paleomeander is greater than 2.4 m. The auger soundings revealed the presence of two main

180 units. The uppermost unit is comprised of topsoil, which overlies a layer of loam containing a

181 significant proportion of gravel and sand in the eastern part of the reference profile. A clayey

182 layer, the bottom of which was not reached in the deepest portion of the paleochannel, is

183 situated below this unit. In some soundings, the clayey facies contains layers of peat (PTA,

184 04, 05, 06, 08, and 09, in Figure 4).

185   The identification of the Holocene clay infilling along this reference profile was

186   confirmed by measuring several and overlapping ERI profiles (24 m common), along the

187   reference transect. For this, a Wenner-Schlumberger array was selected, with 48 electrodes

188   positioned at a 1 m spacing for the first 340 m, and a 0.5 m spacing thereafter.

189   The ERI cross-section (Figure 5) is produced using a dataset of more than 5000

190   measurements. A Wenner-Schlumberger reciprocal array was used, which provides a good

191   compromise between lateral and depth sensitivities (Furman et al, 2003; Dahlin and Zhou,

192   2004).   In order to estimate the interpreted resistivity distribution, the resulting apparent

193   resistivity sections were processed by means of inverse numerical modeling using the

194   Res2dinv software (Loke et al., 2003) with its default damping parameters, and the robust

195   (L1-norm) method. Following a total of 7 iterations, the resulting ERI profiles had an rms

196   error of 0.48% and 0.93%, for the case of the 1 m and 0.5 m electrode spacings, respectively.

197   The resistivity cross-section reveals two main units: an uppermost conductive unit

198   with a resistivity below 20 Ωm, corresponding to a clayey matrix, and a second, more

199   resistive unit with a resistivity greater than 60 Ωm, associated with a medium/coarse-grained

200   silty horizon. The auger soundings are always achieved by a refusal, which is most likely due

201   to the fact that they had reached the resistive second unit. When compared to the analysis

202   achieved using auger soundings, the electrical properties of the topsoil/loam formation appear

203   to be merged with the clayey formation, with the exception of the western portion of the

204   cross-section, which has significant sand and gravel content. This outcome could also be due

205   to the finer spatial resolution of the ERI measurements (electrode spacing of 0.5 m). It is

206   worth noting that the current sensitivity issue associated to the topsoil/loam identification

207   could have probably been overcome with a gradient or a multiple gradient array, without

208   significant loss in DOI (Dahlin and Zhou, 2006).

3.2 EMI surveys and calibration

EMI surveys were carried out using a CMD explorer (GF instruments), at 1-meter height above the ground, with vertical (HCP, horizontal co-planar) and horizontal (VCP, vertical co-planar) magnetic dipole configurations. The CMD explorer operates at 10 kHz, and allows simultaneous measurements to be made with three pairs of Tx-Rx coils (unique Tx coil), using a single orientation (T-mode). Three different offsets were used between the centers of the Tx and the Rx coils, namely, 1.48 m, 2.82 m and 4.49 m, each corresponding to a distinct DOI (approximately 2.2 m, 4.2m, 6.7 m for HCP respectively, and 1.1 m, 2.1 m, 3.3 m for VCP respectively). As the VCP and HCP surveys were made separately in continuous mode (0.6 s time step), slightly different sampling intervals were used. In addition, GPS reception difficulties led to several gaps in the VCP and HCP surveys. It was thus important to carefully evaluate these shortcomings, before merging the HCP and VCP datasets prior to the inversion. As the CMD allows the user to export raw out-of-phase data (including the factory calibration only), no pre-processing is needed to obtain the value of the ratio between the secondary and primary magnetic field amplitude.

Apparent electrical conductivities measured using EMI are particularly sensitive to the orientation of the device, the height above the ground at which the EMI system is setup during the survey, and the 3D variability of the EC. In addition, for the interpretation of the measurements, the ground is assumed to be horizontally layered at any given location, even for the smallest dipole offset. It is worth noting that even if the orientation (vertical or horizontal) and height of the dipole are initialized at the beginning of each survey, variations of orientation and height of the EMI device inevitably occurs and add noise to the measurements.

232   In order to improve absolute (not relative) evaluation of EMI data, in situ calibration

233   of EMI data is important. Ideally, calibration must be performed for several heights and over a

234   perfectly known half space of which electromagnetic properties span over a representative

235   range of EC_a values. For the CMD instrument, calibration factors are provided by the

236   manufacturer for 0 (laid on ground) and 1 m heights. However those factors are valid for a

237   given EC_a range and are dependent on the prospection height (which is never exactly 1 m).

238   This height effect, as mentioned above, has a relative stronger influence on the shortest

239   offsets; consequently, to improve the absolute estimation of EC_a, it is important to have a

240   reference zone where the ground is very well constrained. In order to obtain deeper

241   information than obtained with the hand-made auger soundings, an ERI prospection has been

242   carried out; the inversed ERI section provides reference and absolute values of the local

243   resistivities and can be used in the calibration process as described in Lavoué et al. (2010). It

244   is worth noting that other in situ ways of calibration could be performed (e.g. Delefortrie et

245   al., 2014), particularly, using the theoretical response of a metallic and non-magnetic sphere

246   (Thiesson et al., 2014).

247   During the field data acquisition we faced several difficulties that prevent us to do a

248   CMD profile exactly on the reference profile. Actually, the EMI data used for the calibration

249   have been taken from the mapped data closest to the reference profile. This has led to several

250   positioning and alignment errors because: (1) the EMI data do not exactly cross the reference

251   profile; (2) the EMI data are irregularly spaced along the ERI profile; (3) the orientation of the

252   CMD device was not exactly the same, for each measurement retained for the calibration;

253   and, (4) the height above the surface is changing constantly during the acquisition (less than

254   10-20 cm).

In order to compute the EC_a of a layered ground, based on measurements made using a horizontal or vertical magnetic dipole configuration, we used the well-known electromagnetic analytical solution for cylindrical model symmetry, given by (Wannamaker et al., 1984; Ward and Hohmann, 1988; Xiong, 1989). However, in the case of thin layers or high frequency content, convergence problems can be encountered in the numerical integration of the corresponding oscillating Bessel functions. At frequencies below 100 kHz, as in the case of the present study, the numerical filters developed by Guptarsarma and Singh (1997) were found to provide an efficient solution to this problem. The inversion scheme developed by Schamper et al. (2012) was used to invert the EMI measurements. For each offset and dipole orientation, a linear relationship (shifting and scaling) is determined between each measured EC_a and the EC_a estimated from the resistivity models (derived from the ERI panel, Figure 6). Once the calibration is done, the new EMI inversion matches the ERI used for the calibration which illustrates the validity of the procedure. Despite the linear relationship assessed between the EMI and ERI resistivities, several non-linear operations are applied: (1) ERI local 1D models along the profile are used to simulate EMI measurements; (2) EMI field data are then fitted (linearly) to those simulations using a non-linear optimization procedure to estimate calibration factors; (3) finally the calibrated/shifted data are inverted with a non-linear forward modeling. Each of the previous operations implies a necessary check to ensure that the calibration process has been correctly applied. Step (3) does not guarantee that estimated interfaces will match the ERT interfaces (1) if the fixed/chosen resistivities are not correct, or (2) if EMI does not integrate the ground in the same way as the ERI in case of strong anisotropy, which seems not to be the case here, since a good match is obtained.

The correlation coefficients are comprised between 0.5 and 0.7. Such values can be explained by several sources of errors in the estimation of the EMI apparent conductivities

279 along the reference profile: (1) the differences in the location between the EMI measurements

280 used for the calibration and the ERI profile; (2) the fact that the one dimensional model used

281 for the EMI modeling is extracted from the inversed 2D resistivity section; and, (3) the

282 difference of sensitivity between the ERI and EMI data. The regressions indicate the need of a

283 stronger correction for the VCP configuration than for the HCP configuration. The scaling

284 correction decreases as a function of offset, particularly for the HCP, which can be explained

285 by the fact that small offsets are more sensitive to positioning and orientation errors, as well

286 as to natural near-surface variabilities.

287 **3.3 EMI inversion parameters**

288 Once the calibration process is completed, the corrected, apparent HCP and VCP

289 conductivities are inverted, following their interpolation (by kriging) onto the same regular

290 grid. The ERI results indicate a two-layer model (but do not highlight the topsoil), while the

291 auger sounding show a topsoil layer of a few decimeters thickness above the conductive

292 formation. Consequently, a three-layer model seems reasonably justified all over the site

293 during the inversion process to represent the studied area: a resistive topsoil, a conductive

294 clayey filling, and a resistive sand/gravel layer. The resistivity of each layer corresponds to

295 the peak values of the bimodal histograms of the reference 1-meter-spaced ERI profile, as

296 shown in Figure 7. The topsoil EC derived from the half-meter-spaced ERI profile in the

297 western portion is found to be very similar to the EC of the resistive layer inferred from the

298 1m-spaced ERI profile: thus, the first and third layer EC are considered to be equal. This leads

299 to the following model for the mean EC of the three layers: $\sigma_1 = 13$ mS/m; $\sigma_2 = 72$ mS/m; σ_3

300 $= 13$ mS/m. It should be noted that the CMD explorer is operated at a single frequency (10

301 kHz). The sounding height was taken to be 1 m for all the field measurements.

302 It is worth noting that the 3-layer model chosen instead of a 2-layer model, all over the site,

303 could be questionable. Letting the inversion process decide between a 3 or 2-layer model

304 could have been an option. In the present case, the difference between a 2-layer or 3-layer

305 model is clearly negligible where the interpreted thickness of the topsoil (for the 3- layer

306 model) is less than a few decimeters. For such low thicknesses the topsoil can be considered

307 as non-existent considering the acquisition geometry and settings of the CMD explorer.

308 Figure 8 shows the inverted thicknesses of the first and second layers, and the data residual

309 for the HCP (3 offsets), the VCP (3 offsets), and the combined HCP and VCP conductivities

310 (6 apparent values). The standardized root-mean-squared residual (SRMR) for N independent

311 measurements is given by:

$$SRMR = \sqrt{\frac{\sum_{i=1}^{N} \left(\frac{d(i) - d_{meas}(i)}{std(i)}\right)^2}{N}} \tag{1}$$

312 Where N is the number of data points, d is the forward response of the estimated model at the

313 end of the inversion, d_{meas} contains the data, and std is the standard deviation of the data. The

314 standard deviation std was estimated from repeated measurements at several locations, as

315 1 mS/m (with a minimum error of 5%).

316 **3.4 EMI results**

317 **3.4.1 General trend**
318 The layer thickness inversion was performed using three different datasets: (1) the HCP

319 dataset, (2) the VCP dataset, and (3) the combined HCP and VCP dataset (Figure 8).

320 Whatever the dataset used for the inversion, the thickness computed for the topsoil

321 formation (indicated by *"Thickness 1"* in Figure 8) is globally very small (blue), whereas that

322 computed for the conductive infilling (indicated by *"Thickness 2"*) has a significantly higher

323   value (red), and *vice versa*. Although it varies in thickness, the conductive layer formation

324   spans most of the survey area, whereas the resistive topsoil formation varies mainly in two

325   distinct locations: (1) the south-western limit of the surveyed area, where it reaches a depth of

326   2 m; and, (2) the mid-northern portion of the surveyed area, where its thickness never exceeds

327   0.6 m. In addition, very small scale topsoil formations are scattered over the surveyed area. In

328   all places where the estimated thickness of the first layer is less than 20 cm, the topsoil can be

329   considered as inexistent and a 2-layered model is enough to explain EMI data. Nevertheless,

330   all of the observed topsoil formations appear to be correlated with a local increase in data

331   residual. The thickness of the conductive infilling lying below the topsoil formation ranges

332   between 0 m, in the south-western portion of the studied zone, and its maximum value of

333   almost 2 m at the center of the map.

334   The VCP mode increases the measured thickness of the shallowest portions of the

335   topsoil layer, whereas the HCP mode tends to negate this layer over most of the surveyed area

336   (central part), where it is not extremely thick. This tendency appears to be correlated with a

337   slight increase in the thickness of the second conductive layer.

338   The inversion of all data, in the form of a single dataset, appears to lead to a mixture of

339   the properties inherent to each of the constituent datasets. This outcome is particularly

340   noticeable in the case of the topsoil formation, where certain structures retrieved by both

341   datasets are emphasized with respect to structures that are present in only one or the other of

342   these.

343   **3.4.2 Internal variability**

344   In addition to strong meander wavelength variations, each dipole orientation reveals different

345   level of heterogeneities in the material present in the conductive infilling, as well as the

346   topsoil. Concerning the material close to the surface (< 2 m), this variability is clearly

347 illustrated by the auger soundings, whereas the conductive unit identified by the ERI section

348 is considerably more complex. In simple terms, the thickness of the conductive material tends

349 to decrease, wherever the silty and sandy material reaches the surface.

350 It should be noted that the inversions observed for each dipole orientation are not

351 systematically preserved in the inversion produced by combining the data from both dipole

352 orientations. This result indicates that in the present context, each orientation is

353 complementary, and contributes a specific set of information. This is particularly relevant in

354 the northern portion of the studied area, where the thickness of the first resistive layer is more

355 variable when it is measured with the horizontal dipole configuration (VCP), than with the

356 HCP configuration.

357 The data residual has numerous peaks in the south-western portion of the study zone.

358 In this zone, the resistive topsoil reaches a thickness of 1 m, leading to EMI measurements

359 with a lower sensitivity (and thus lower signal to noise ratio - SNR). The combined

360 HCP&VCP data inversion naturally leads to the occurrence of higher values of data residual

361 than in the case of the individual HCP or VCP inversions. Indeed, it is difficult to compare the

362 data residual maps between the three proposed datasets (i.e. HCP alone, VCP alone and both)

363 as the physical contribution associated to each dataset inversion results is related to the couple

364 dataset & model used for the inversion. HCP and VCP modes do not integrate the ground in

365 the same way exactly. If the ground within the footprint of the EMI system is a bit far from a

366 tabular model, then the interpretation with local 1D models can be more difficult with both

367 data sets combined than with only one of the two sets analyzed. The difficulty to invert the

368 HCP and VCP datasets jointly also arises from the fact that: (1) the locations of the soundings

369 between the two surveys are not exactly the same as the modes cannot be acquired at the same

370 time; (2) the heights varies differently; and (3) the pitch and roll are not constant. For those

371 last two points one could imagine the monitoring of these "flight" parameters to correct the

372 data, which is routinely done for airborne electromagnetic surveys. But this feature does not

373 exist at the present time for ground based EMI devices.

374   **4. Discussion**
375

376 In the present study, the outcomes of ERI and EMI surveys integrate quite satisfactorily the

377 lithological information provided by the auger soundings, but have not yet been checked with

378 exhaustive hydrological information. During the presented geophysical campaign (low water

379 period), the water level measured from PTA02 to PTA04 and from PTA11 to PTA13

380 locations indicate a groundwater situated at 1 m depth, roughly at the interface between the

381 clay infilling and the upper geological unit (Figure 4). In the survey area the water table could

382 rise close to the surface at high water periods, which implies that the conductivity of the

383 topsoil/loam formation should increase. In the closest piezometer located 1 km west from the

384 prospected site, the water table was situated at 70 cm below the surface. The EC measured in

385 the same piezometer in 2011 was 640 µS/cm (12Ωm) and showed a seasonal variation of the

386 water table of approximately 60 cm (Voies Naviguables de France (VNF) tech. report, 2011).

387   The clay infilling is then always saturated while the topsoil/loam upper unit is almost

388 never dry. Even significant changes in the degree of saturation of the topsoil/loam formation

389 would hardly allow the value of its resistivity to lower down to the resistivity of the clay

390 infilling (~10-20 Ω.m) estimated from the histogram (Figure 7). Consequently, if the

391 thickness of the topsoil/loam formation is significantly larger than a few decimeters, the

392 presence of the water table at the surface does not challenge the three layer model assumption

393 based on the lithological boundaries.

394   From a hydrogeological modeling perspective, one of the most important issues is the

395   assessment of the constitutive relationship that links EMI/ERI electrical

396   conductivity/resistivity to hydrodynamic properties (i.e. the permeability) because of the

397   difficulty to discriminate the bulk conduction from the surface conduction mechanism. In the

398   present case, a sample located at PTA12 and at a depth between 140 and 160 cm, show major

399   peaks of calcite and quartz, significant peaks of illite-montmorillonite, and small peaks of

400   kaolinite. The clayey infilling corresponds to a saturated marl sediment containing 20-30% of

401   clay and 50-60% carbonate. The high amount of carbonate originates from the weathering of

402   the chalky cretaceous limestones that outcrop on the borders of the alluvial plain. As the

403   salinity is low and the clay content significant, the electrical conductivity of the clayey

404   infilling is essentially driven far more by the surface conductivity than by the pore water

405   conductivity. As it is not the case for the first decimeter of topsoil/loam, it could be another

406   argument that reinforces the pertinence of the three layer model assumption for the inversion

407   process.

408   From a more general perspective, EMI calibrated with ERI and auger soundings

409   contributed to a better characterization of the geometry and variability of this paleomeander.

410   The results reveal a complex cross-sectional geometry of the conductive clayey layer,

411   featuring from the south-west to the north-east: (1) a sharp contact to the south-west with a

412   resistive sand and gravel layer; (2) a roughly constant thickness of 2 meters of the conductive

413   layer, extending over more than 200 m; (3) a decrease of the thickness of the conductive layer

414   (~ 0.5 m) related to the raising of the gravely substrate, over a length of ~ 100 m; and, (4) an

415   increase of the conductive layer to the north-east. Unfortunately, the contact of the conductive

416   layer with the resistive layer to the north-east was not captured due to the limited extent of the

417   surveyed area. It is thus difficult to conclude if the paleomeander is restricted between PTA03

418 and PTA10, with a mean depth of 2 m and a width of 250 m, or if the former channel was

419 wider (> 350 m) with a shallower part associated to sand/gravel bars. It is also not excluded

420 that several (2 or 3) small channels were active during low water stages within a larger

421 "bankfull channel", producing local incision of the bed. Nevertheless, and compared to the

422 modern Seine river (~ 50 m wide, up to 5 m deep), this paleochannel attributed to the Late

423 Glacial/Preboreal period shows a larger width, and a significantly larger width-to-depth ratio.

424 These differences are attributed to different paleohydrological and paleoclimatic conditions,

425 with larger water discharges, larger and coarser solid fluxes, and less cohesive soils in the

426 absence of developed vegetation.

427 From a hydrogeological perspective, the paleo-meanders of the Late Glacial/Preboreal

428 period are filled with large but relatively thin (2 m) mudplugs compared to the alluvial plain

429 thickness (6 to 8 m), which should produce little impact on the groundwater flow. However,

430 this should be confirmed by numerical modeling. The study should be extended to paleo-

431 meanders attributed to different climatic periods of the Holocene, which present different

432 morphologies and aspect ratios.

433 **5. Conclusion**
434

435 We presented the results of the geophysical investigations of a paleochannel in the Bassée

436 alluvial plain (Seine Basin, France). The location of this paleochannel and its geometry,

437 suggested by a LIDAR campaign, have been accurately mapped using a multi-configuration

438 (various offsets and orientations) electromagnetic induction device.

439 In order to correct the drift and factory calibration issues arising from EMI

440 measurements, a calibration procedure was implemented, based on the use of a linear

441 correction with ERI inversion results and auger soundings. The shifting and scaling of EMI

442 HCP and VCP measurements was made for the three available offsets (1.48, 2.82 and

443 4.49 m), at a frequency of 10 kHz. Six apparent conductivities allowed the inversion of a

444 reliable three-layer model, comprising a conductive filling with an EC equal to 72 mS/m

445 below the topsoil, and a resistive substratum having an EC equal to 13 mS/m. The

446 conductivities of the three-layer model were adjusted using the bimodal histogram distribution

447 of the reference ERI profile. The inverted thicknesses are characterized by a significant

448 internal variability in the conductive filling and the topsoil, associated with the paleochannel

449 geometry.

450 The joint inversion of multi-offset HCP and VCP configurations leads to a very

451 interesting result, in which the internal variability description is considerably enhanced. We

452 believe that multi-configuration EMI geophysical survey carried out at an intermediate scale

453 should provide a great complement to TDR (Time Domain Reflectometry) for a quantitative

454 and physical calibration of remote sensing soil properties and moisture content. Combined

455 multi offset VCP and HCP prospections could significantly improve the accuracy of

456 hydrogeological modeling by potentially providing a hydrogeological picture of the first

457 meters sedimentary setting in terms of lithological distribution; but it would also lead to a

458 substantial increase in survey costs with the instruments currently available on the market.

459

460

461 **6- Data availability**
462 In order to access the data, we kindly ask researchers to contact the corresponding author.

463

7- Acknowledgement

This research was supported by the PIREN Seine research program (2015-2019). We extend

our warm thanks to Christelle Sanchez for her participation in the geophysical survey and to

Laurence LeCallonnec for carrying out the XRD experiment.

8- References

Antoine, P., Coutard, J.-P., Gibbard, P., Hallegouet, B., Lautridou, J.-P., and Ozouf, J.-C.:

The Pleistocene rivers of the English Channel region, Journal of Quaternary Science, 18, 227–

243, 2003.

Benech, C., Lombard, P., Rejiba, F., and Tabbagh, A: Demonstrating the contribution of

dielectric permittivity to the in-phase EMI response of soils: example of an archaeological site

in Bahrain, Near Surface Geophysics, 14(4), 337-344, 2016.

Berger, G., Delpont, G., Dutartre, P., and Desprats, J.-F.: Evolution de l'environnement

paysager de la vallée de la Seine - Cartographie historique et prospectives des explorations

alluvionnaires de la Bassée, French Geological Survey (BRGM) report R 38 726, 39 p., 1995.

Caillol, M., Camart, R., and Frey, C.: Synthèse bibliographique sur la géologie, l'hyrogéologie

et les ressources en matériaux de la région de Nogent-sur-Seine (Aube), French Geological

Survey (BRGM) report 77 SGN 303 BDP, 108 p, 1977.

Dahlin, T. and Zhou, B.: A numerical comparison of 2D resistivity imaging with 10 electrode

arrays, Geophysical prospecting, 52(5), 379-398, 2004.

Dahlin, T. and Zhou, B.:Multiple-gradient array measurements for multichannel 2D resistivity

imaging, Near Surface Geophysics, 4(2), 113-123, 2006

Delefortrie, S., De Smedt, P., Saey, T., Van De Vijver, E., and Van Meirvenne, M.: An efficient calibration procedure for correction of drift in EMI survey data, Journal of Applied Geophysics, 110, 115-125, 2014.

Deleplancque, B. : Caractérisation des hétérogénéités sédimentaires d'une plaine alluviale : Exemple de l'évolution de la Seine supérieure depuis le dernier maximum glaciaire, PhD Thesis, PSL Research University – Paris, 273 p., 2016.

De Smedt, P., Van Meirvenne, M., Meerschman, E., Saey, T., Bats, M., Court-Picon, M., De Reu, J., Zwertvaegher, A., Antrop, M., Bourgeois, J., and De Maeyer, P.: Reconstructing palaeochannel morphology with a mobile multicoil electromagnetic induction sensor, Geomorphology, 130, 136-141, 2011.

Everett, M. E.:Theoretical developments in electromagnetic induction geophysics with selected applications in the near surface, Surveys in geophysics, 33(1), 29-63, 2012

Fitterman, D.V., Menges, C.M., Al Kamali, A.M., and Jama, F.E.:Electromagnetic mapping of buried paleochannels in eastern Abu Dhabi Emirate, UAE, Geoexploration, 27, 111-133, 1991.

Flipo, N., Mouhri, A., Labarthe, B., Biancamaria, S., Rivière, A., and Weill, P.: Continental hydrosystem modelling: the concept of nested stream-aquifer interfaces, Hydrology and Earth System Sciences, 18, 3121–3149, 2014

Friedman, S. P.: Soil properties influencing apparent electrical conductivity: a review, Computers and electronics in agriculture, 46(1), 45-70, 2005.

505 Furman, A., Ferré, T., and Warrick, A. W.: A sensitivity analysis of electrical resistivity

506 tomography array types using analytical element modeling, Vadose Zone Journal, 2(3), 416-

507 423, 2003.

508 Guptasarma, D. and Singh, B.: New digital linear filters for Hankel J0 and J1 transforms,

509 Geophysical Prospecting, 45(5), 745–762, 1997.

510 Jordan, D.W. and Prior, W.A.: Hierarchical Levels of Heterogeneity in a Mississippi River

511 Meander Belt and Application to Reservoir Systems: Geologic Note, AAPG Bulletin, 76(10),

512 1601-1624, 1992.

513 Huang, H.: Depth of investigation for small broadband electromagnetic sensors, Geophysics,

514 70 (6), G135–G142, 2005

515 Lavoué, F., Van Der Kruk, J., Rings, J., André, F., Moghadas, D., Huisman, J. A., Lambot, S,

516 Weihermüller, L., Vanderborght, J., and Vereecken, H.: Electromagnetic induction calibration

517 using apparent electrical conductivity modelling based on electrical resistivity

518 tomography, Near surface geophysics, 8(6), 553-561, 2010.

519 Loke M.H., Acworth I., and Dahlin T: A comparison of smooth and blocky inversion methods

520 in 2D electrical imaging surveys, Exploration Geophysics, 34, 182–187, 2003

521 Mégnien, F. : Possibilités aquifères des alluvions du val de Seine entre Nogent-sur-Seine et

522 Montereau, incluant la carte géologique et géomorphologique de la Bassée, French Geological

523 Survey (BRGM) report 65-DSGR-A-076, 452 p., 1965.

524 Miall, A.D.: Reservoir Heterogeneities in Fluvial Sandstones: Lessons from Outcrop Studies,

525 AAPG Bulletin, 72(6), 682-697, 1988.

526   Mordant, D. : La Bassée avant l'histoire : archéologie et gravières en Petite-Seine, Association

527   pour la promotion de la recherche archéologique en Ile-de-France, Nemours, 143 p., 1992.

528   Nabighian, M. N. (Ed.): Electromagnetic methods in applied geophysics (Vol. 1), SEG Books,

529   1988a.

530   Nabighian, M. N. (Ed.): Electromagnetic methods in applied geophysics (Vol. 2), SEG Books,

531   1988b.

532   McNeill, J. D.: Electromagnetic terrain conductivity measurement at low induction numbers,

533   Geonics Technical Note TN-6, 1980.

534   Pastre, J.-F., Limondin-Lozouet, N., Leroyer, C., Ponel, P., and Fontugne, M.: River system

535   evolution and environmental changes during the Lateglacial in the Paris Basin (France),

536   Quaternary Science Reviews, 22, 2177–2188, 2003.

537   Rhoades, J. D., Raats, P. A. C., and Prather, R. J.: Effects of liquid-phase electrical

538   conductivity, water content, and surface conductivity on bulk soil electrical conductivity, Soil

539   Science Society of America Journal, 40(5), 651-655, 1976

540   Spies, B. R.: Depth of investigation in electromagnetic sounding methods, Geophysics, 54(7),

541   872-888, 1989.

542   Schamper, C., Rejiba, F., and Guérin, R.: 1D single-site and laterally constrained inversion of

543   multifrequency and multicomponent ground-based electromagnetic induction data —

544   Application to the investigation of a near-surface clayey overburden, Geophysics, 77(4),

545   WB19-WB35, 2012.

546 Simon, F. X., Sarris, A., Thiesson, J., and Tabbagh, A.: Mapping of quadrature magnetic

547 susceptibility/magnetic viscosity of soils by using multi-frequency EMI, Journal of Applied

548 Geophysics, 120, 36-47, 2015.

549 Tabbagh, A.: Applications and advantages of the Slingram electromagnetic method for

550 archaeological prospecting, Geophysics, 51(3), 576-584,1986.

551 Thiesson, J., P. Kessouri, C. Schamper, and Tabbagh A.: About calibration of frequency

552 domain electromagnetic devices used in near surface surveying, Near Surface Geophysics, 12,

553 481–491,2014.

554 VNF (Voies navigables de France), 2011. Etat des lieux de la piézométrie de la petite Seine,

555 Technical Report (in french), 58p.

556 Wannamaker, P. E., Hohmann, G. W., and Sanfilipo, W. A.: Electromagnetic modeling of

557 three-dimensional bodies in layered earths using integral equations, Geophysics, 49, 60–74,

558 doi: 10.1190/1.1441562, 1984.

559 Ward, S. H. and Hohmann, G. W.: Electromagnetic theory for geophysical applications, In

560 Electromagnetic methods in applied geophysics, Vol. 1 : Theory, pp. 131–311. Nabighian,

561 M.N., 1988.

562 Xiong, Z.: Electromagnetic fields of electric dipoles embedded in a stratified anisotropic

563 earth, Geophysics, 54, 1643–1646, doi: 10.1190/1.1442633, 1989.

564

565   **Figures**

566
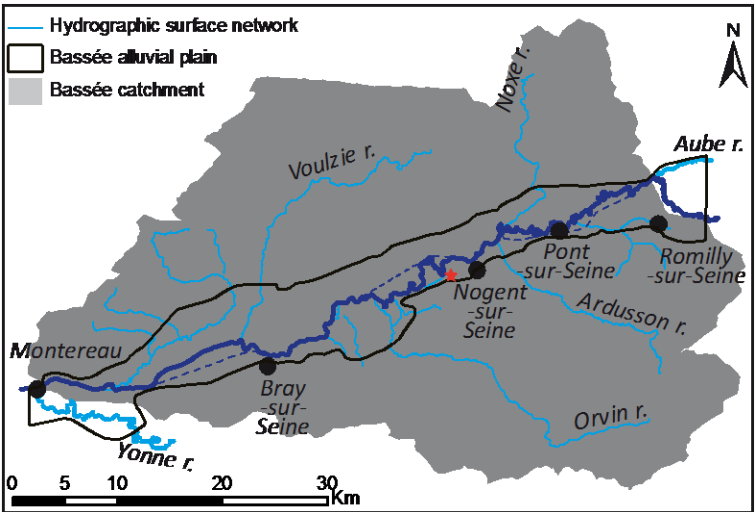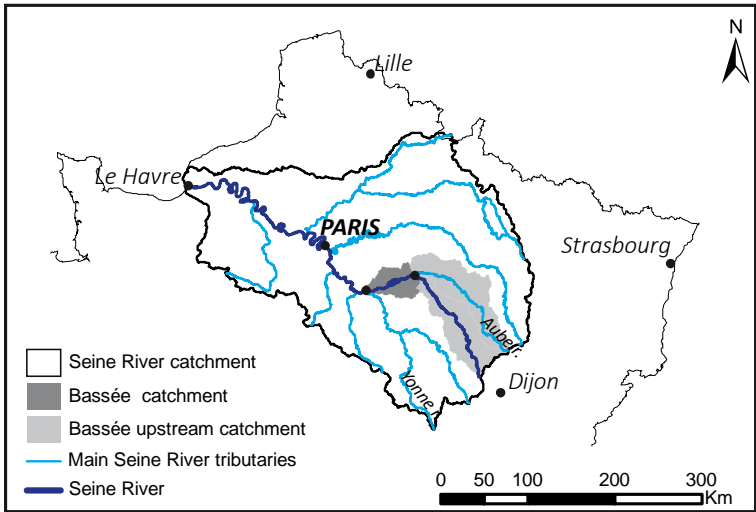
567   Figure 1: Maps of the Seine catchment (top) and the Bassée alluvial plain (bottom).

568

Figure 2 : LIDAR map of the study area, showing the contemporary location of the Seine
River, together with the narrow and wide paleochannel interpretations.

571

572
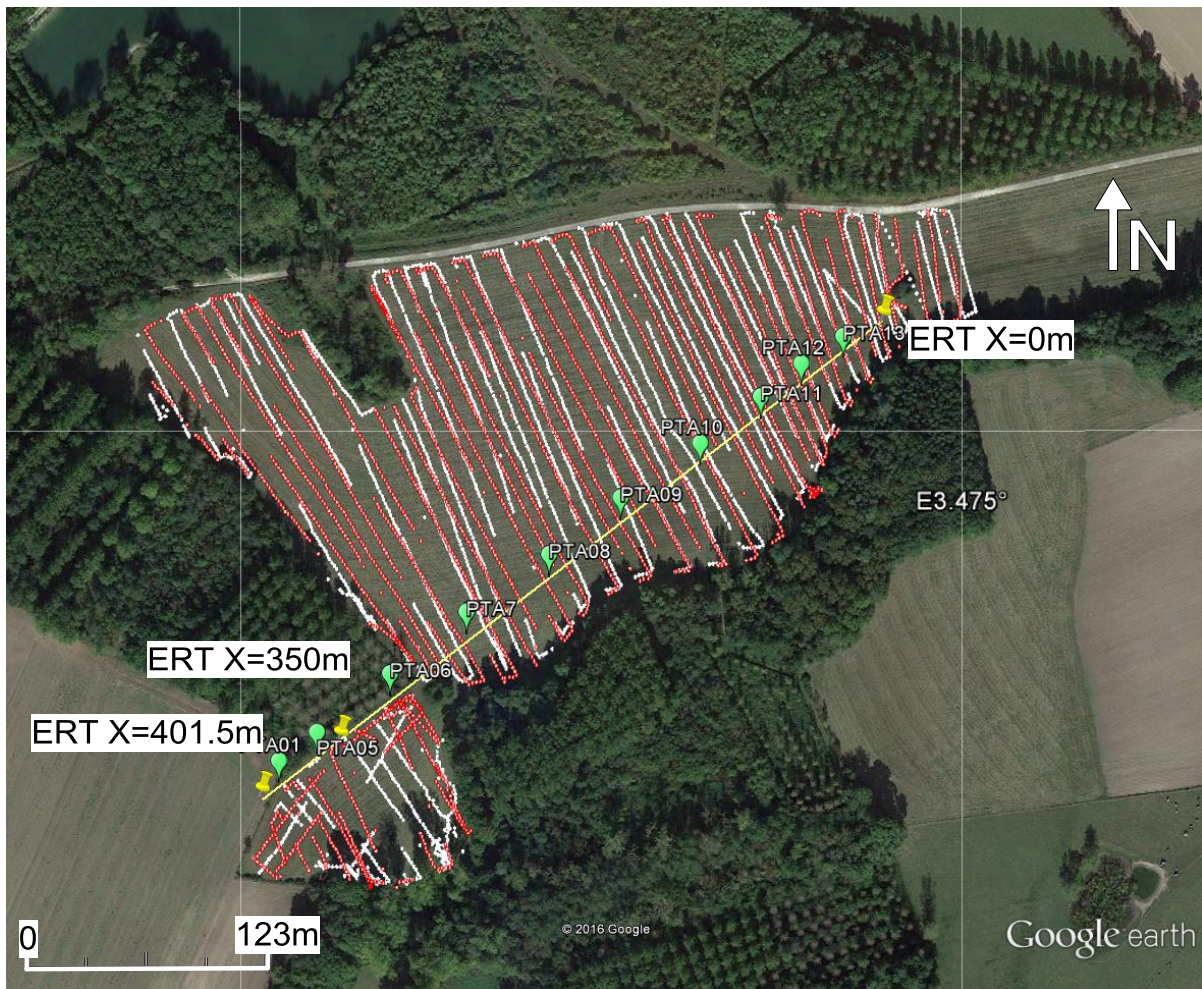
573   Figure 3: Map of the surveyed area, showing the locations of the VCP (red) and HCP (white)

574   measurements (GPS issues explain the holes within the lines). The reference (ERI) profile,

575   recorded with a Wenner-Schlumberger configuration using 1 m electrode spacing between 0

576   and 350 m, and a 0.5 m electrode spacing between 350 m and 401.5 m, is indicated by the

577   yellow line. As green dots, the locations of the hand auger drillings.

578

579
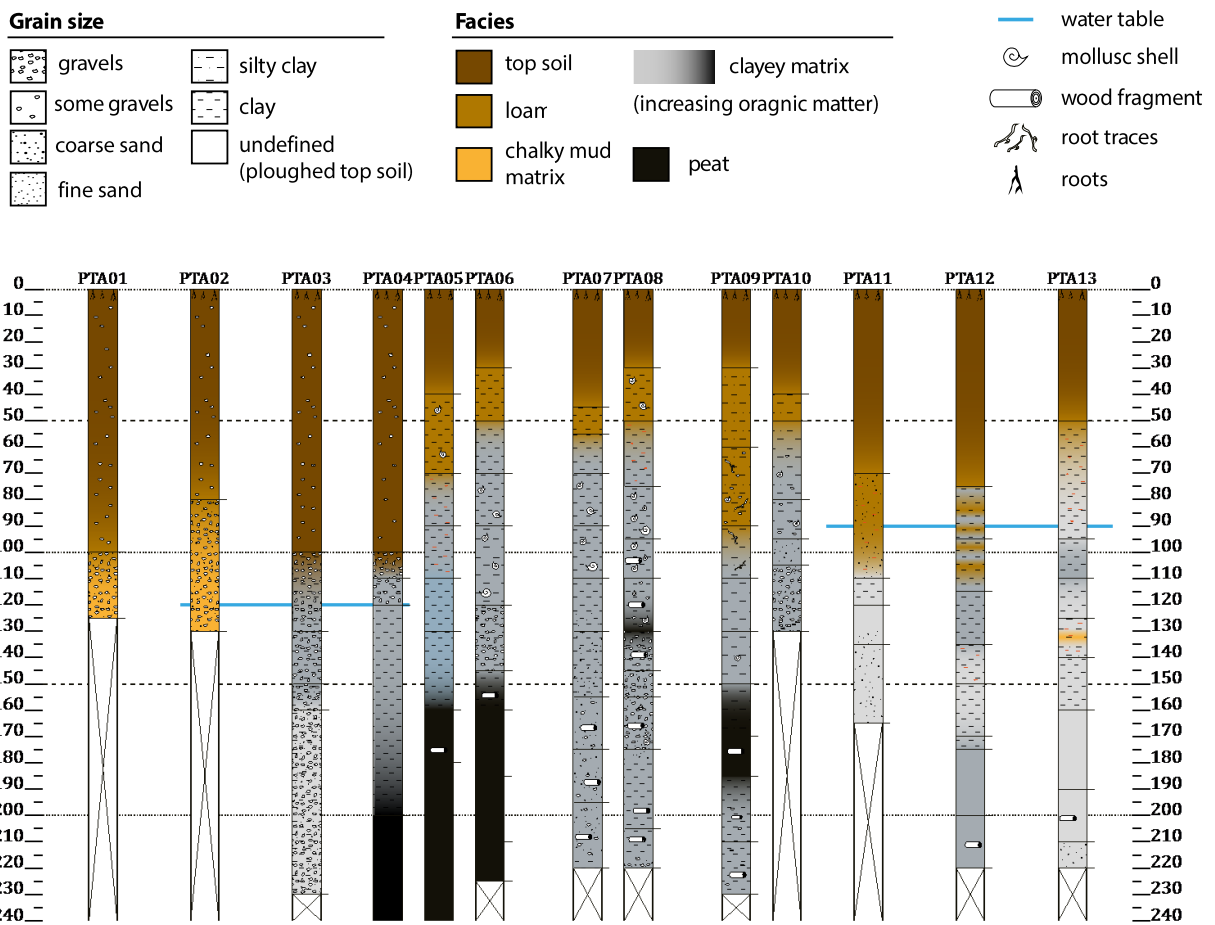
Figure 4: Log of hand auger soundings performed along the reference profile. The position of

each sounding along the ERI profile is shown in Figure 5.

582

583
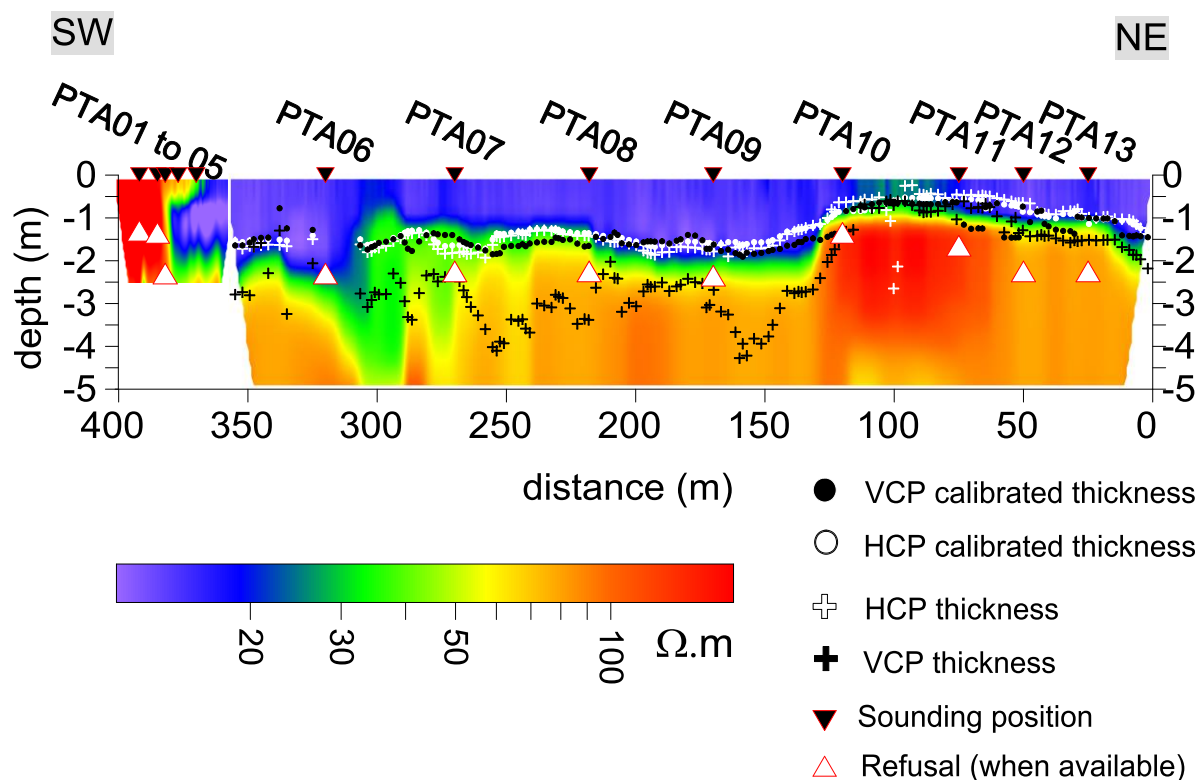
584   Figure 5: Results from the electrical resistivity tomography (ERI) inversion, computed along

585   the reference profile. This section reveals the two main (conductive and resistive) geological

586   units. The markers correspond to the inverted location of the interface (from EMI

587   measurements) between the conductive unit and the substratum, before and after linear

588   calibration (Figure 6). This figure shows that calibration of the raw VCP measurements leads

589   to significant corrections in inverted depth, when compared to the calibration of the HCP

590   measurements.

591

592
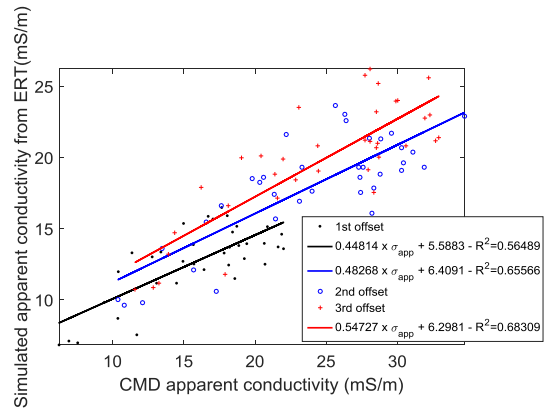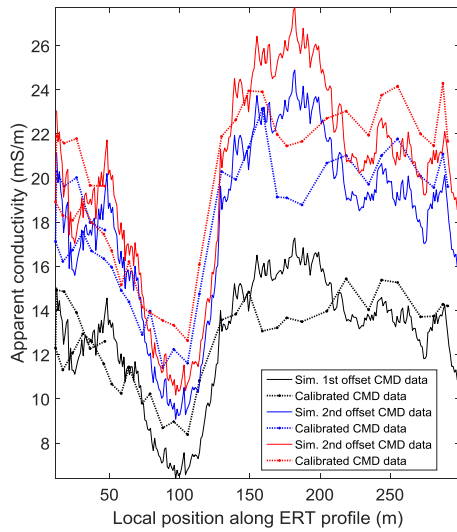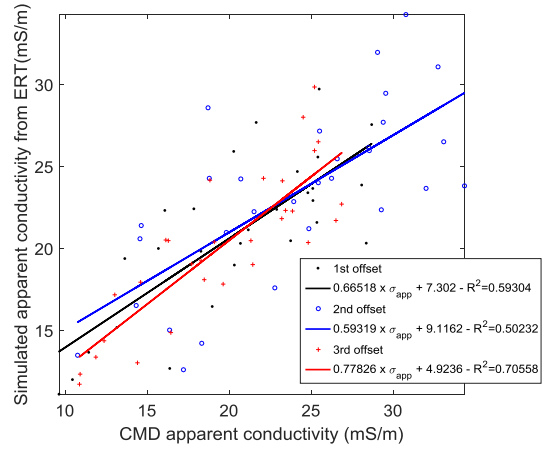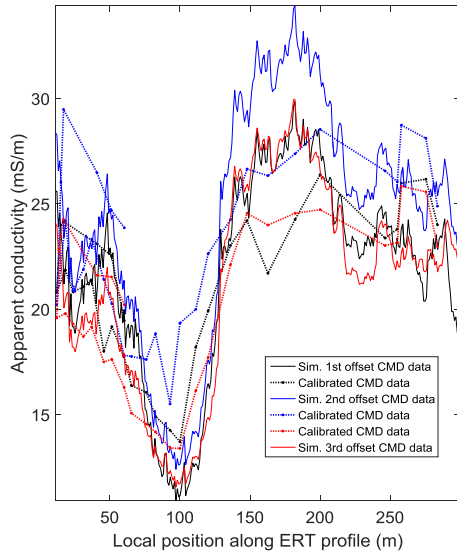
Figure 6: HCP (top) and VCP (bottom) calibration results obtained along the reference profile. Left: the simulated apparent CMD conductivities based on the ERI inversion compared to the calibrated EMI measurements. Right: scatter plots of the measured *vs.* simulated apparent conductivities. The solid lines indicate the corresponding linear regressions.
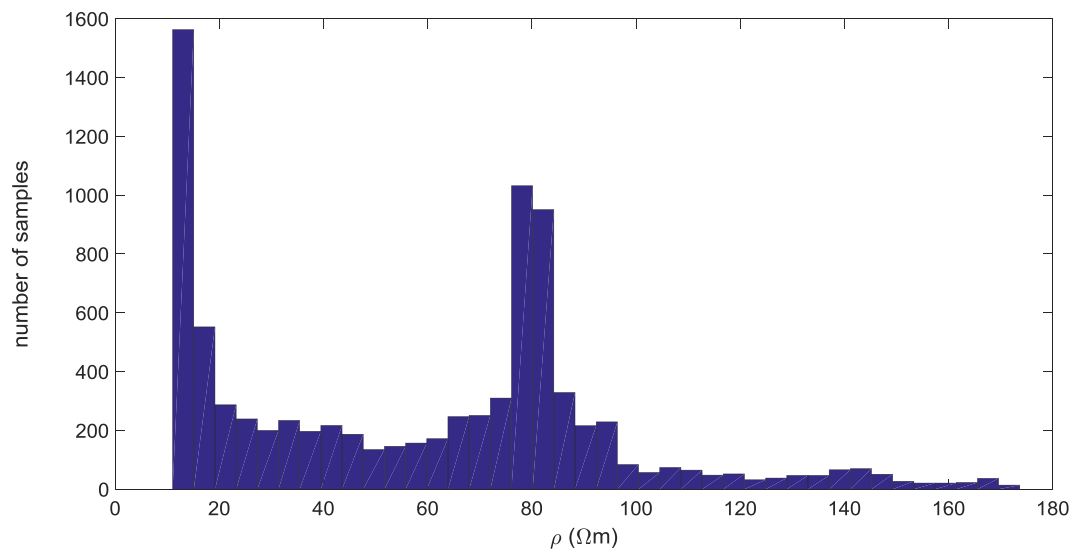
598

599   Figure 7: Histogram of the electrical resistivity values determined for the ERI section shown

600   in Figure 5.

601

602

603

604

605
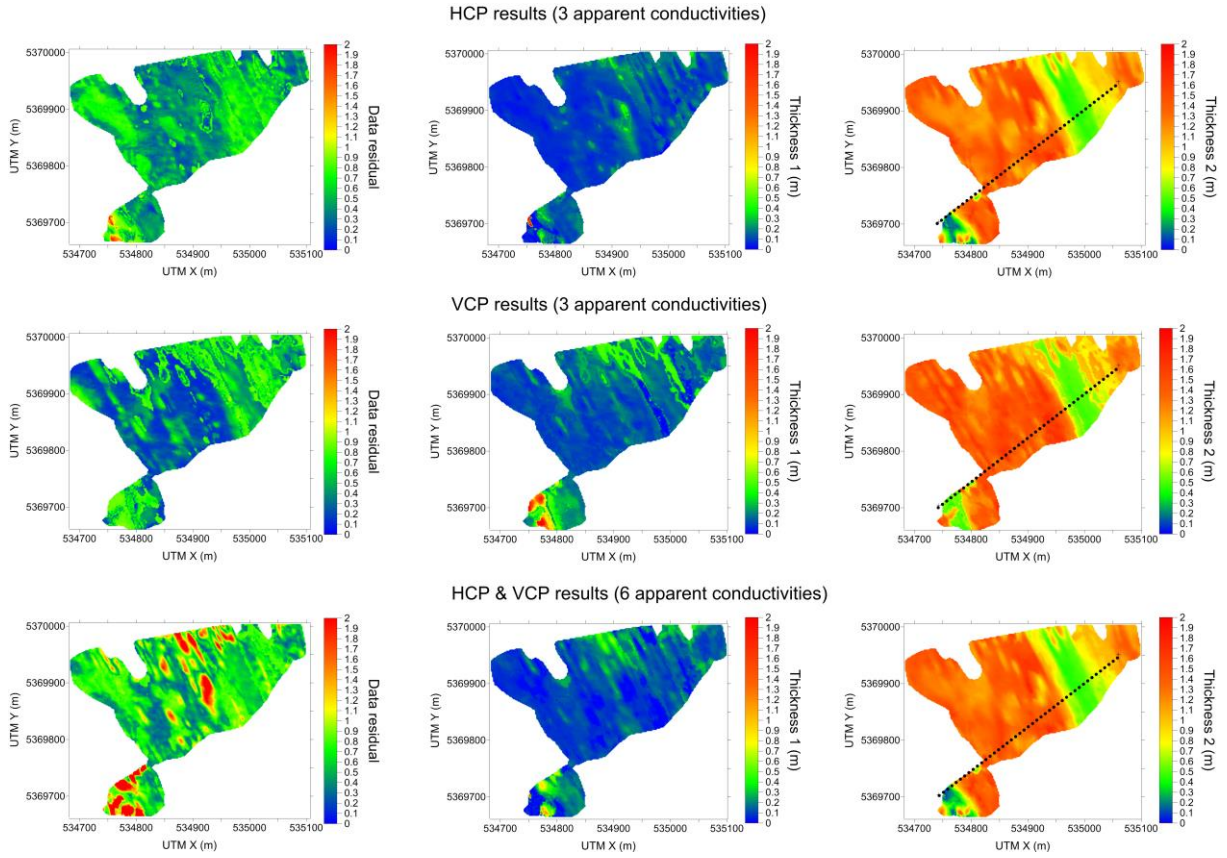
Figure 8: Results of the CMD inversion, including the data residual (left column), for a three-layer model (1: topsoil, 2: conductive filling, and 3: resistive substratum). The thicknesses 1 and 2 correspond to the topsoil and conductive filling, respectively. The prospection height is 1 m. The conductivities are set to $\sigma_1 = 13$ mS/m, $\sigma_2 = 72$ mS/m and $\sigma_3 = 13$ mS/m. A noise level of 1 mS/m on the apparent conductivities was assumed, with a minimum relative error of 5%. The black dashed line indicates the ERI reference profile location.

612